Optimization and Comparison of 1MW-Class PM Motors for Aircraft Propulsion Using Litz Wire and Hairpin Windings

Anh Thanh Huynh, *Member, IEEE;* Hailin Huang, *Member, IEEE;* Jianan Jiang, Tianjie Zou, *Member, IEEE;* David Gerada, *Senior, IEEE;* Tao Yang, *Senior, IEEE;* and Chris Gerada*, *Senior, IEEE*

Power Electronics, Machines and Control Research Institute, University of Nottingham, Nottingham, NG7 2GT, UK

Choosing the right winding technology is key to maximizing power density and efficiency in electric aircraft propulsion. This paper presents a two-level optimization strategy to evaluate Litz wire and hairpin winding configurations in two 1 MW-class PM machines, each with a 5-stage Halbach array and a 72-slot/12-pole configuration. The global optimization (GO) stage analyzes their impact on power density, loss distribution, and efficiency. Results show that hairpin winding increases power density by reducing active mass but suffers from higher AC copper losses. To address this, an updated motor constant (K_m) serves as a fitness function in a Genetic Algorithm (GA) during the local optimization (LO) stage, refining the hairpin winding and stator slot design to reduce losses and enhance efficiency. Finite Element Analysis (FEA) validates the performance and effectiveness of the proposed method.

***Index Terms*— Aircraft Applications, PM machines, Litz Wire, Hairpin Winding, High Power Density, Optimization.**

I. Introduction

Climate change is driving the demand for eco-friendly mobility, with aviation as a fast-growing emitter of greenhouse gases. In 2022, it accounted for 2.4% of global CO_2 emissions, rising faster than other transport sectors [1]. To reduce emissions, the industry is prioritizing the electrification of aircraft propulsion (EAP) to cut energy use, emissions, and noise. EAP focuses on advancing electric machines for higher power density (PD), efficiency, and reliability [2], making permanent magnet machines (PMSMs) the preferred choice.

Maximizing the power-to-mass ratio (kW/kg) is crucial for next-generation aircraft propulsion motors, which aim to exceed 20 kW/kg by reducing weight and improving efficiency [2, 3]. Advanced winding technologies, including Litz wire and high-temperature superconducting (HTS) windings, are key to minimizing AC losses and enhancing efficiency in PMSMs [3-10].

Litz wire technology enabled a 1 MW slotless permanent magnet (PM) motor to achieve 23.8 kW/kg with 97.2%-98.3% efficiency [4] and boosted 4 MW propulsion systems to around 20 kW/kg at over 97% efficiency [5]. A 1 MW Inner Rotor Surface Permanent Magnet (IRSPM) machine using Litz wire reached 23.6 kW/kg at 96.9% efficiency [6]. Meanwhile, HTS technology further improved performance, with a 1.4 MW wound-field synchronous machine (WFSM) achieving 16 kW/kg at 98% efficiency [7], a 2.7 MW turbofan-integrated induction machine reaching 13 kW/kg [8], and a 2.5 MW slotless 8-pole generator achieving 24.4 kW/kg at over 99% efficiency [9]. Finally, a 2 MW partially superconducting WFSM with a helical winding and slotless stator attained 14.25 kW/kg at over 98% efficiency [10].

Hairpin windings with rectangular conductors emerge as a superior alternative to traditional random windings in next-generation traction motors, enhancing PD and efficiency in electric vehicles. Their high slot fill factor lowers DC resistance and losses while improving cooling and current density [11,12]. However, above 1 kHz, AC losses increase due to skin and proximity effects and circulating currents in unbalanced branches [11,12]. Despite these challenges, research on their application in aircraft propulsion remains limited.

Finite element method (FEM) and optimization techniques enhance PMSM design quality and shorten the design cycle, but fluctuations in design variables or operating conditions can impact performance. Multilevel optimization effectively addresses these parameter variations in complex problems [13]. This paper proposes a two-level optimization strategy to address the challenge of coupled global and local variables in 1 MW-class PM motor design, comparing hairpin windings to Litz wire. First, global optimization (GO) is applied to two 72-slot/12-pole models using Litz wire and hairpin windings to maximize PD and efficiency. The optimization results, including PD, loss distribution, and efficiency, are thoroughly evaluated and compared, with additional analysis of AC loss effects in hairpin windings at high frequencies. Next, to reduce AC losses in hairpin windings and enhance efficiency, an updated motor constant (K_m) is developed and used as a fitness function in a Genetic Algorithm (GA) during the local optimization (LO) stage to refine hairpin winding and stator slot design. Finally, the effectiveness of the proposed method is validated through Finite Element Analysis (FEA).

II. Design Consideration and Optimization

A. Analysis Models

In aerospace, minimizing mass is prioritized over volume. Current 1 MW aircraft propulsion systems achieve an active PD of 20-25 kW/kg. This study aims for a PD above 25 kW/kg and 98% efficiency for a 1 MW machine at 10,800 rpm. Two 1 MW-class PM machines, both with a 5-stage Halbach array and 72-slot/12-pole configuration (Fig. 1), are investigated, comparing Litz wire and hairpin winding configurations' impact on PD and efficiency. Both models share identical stator and rotor core dimensions, with the active length varying by winding type. The stator material is Vacoflux 48 with a 0.05mm thickness. Table I lists key parameters, material properties, and design targets. The Litz wire configuration minimizes AC loss in copper, so its AC loss is excluded, while the hairpin

winding's AC loss is evaluated using FEA software [12].

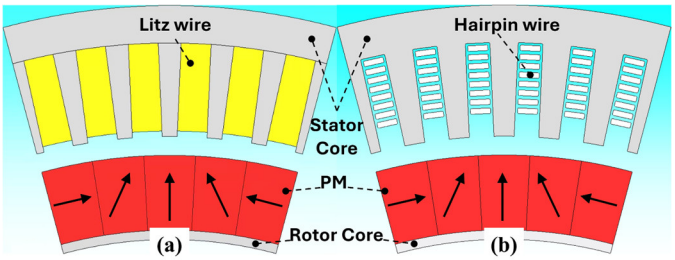

Fig. 1. Models of 1MW class PM machines with different winding configurations. (a) Litz wire, (b) Hairpin winding.

TABLE I
SPECIFICATIONS AND PARAMETERS OF 1 MW CLASS PM MACHINES

Item	Litz wire	Hairpin
Stator Outer/Inner Diameters	345/275 mm	
Rotor Outer Diameter	265 mm	
Stack Length	106 mm	85 mm
Air-gap length	5 mm	
Number of turns/layers per slot	10 turns	8 layers
Rated speed	10800 rpm	
Rated power	1 MW	
Stator/Rotor materials	Vacoflux 48 0.05 mm/Aluminum	
PM material and Thickness	Recoma 30HE – 20 mm	
DC Bus voltage	800 V	
Active Power Density	>25 kW/kg (active mass)	
Efficiency	>98%	

B. Motor Constant

The motor constant K_m is key to motor sizing, as it defines the torque-power relationship and indicates conversion efficiency, with higher values signifying better energy conversion [14]. It is defined as:

$$K_m = T_e \Big/ \sqrt{I_s^2 R_s} = K_t \Big/ \sqrt{R_{s\_DC}} \tag{1}$$

where K_t is the motor constant, T_e is electromagnetic torque, I_s is peak armature current.

Equation (1) shows that K_m considers only DC copper loss for efficiency evaluation, suitable for round windings like Litz wire. For hairpin windings, AC losses must also be included, with phase AC resistance R_{s_AC} given as:

$$R_{s\_AC} = (1 + \kappa_{skin} + \kappa_{prox}) R_{s\_DC} \tag{2}$$

where κ_{skin} is the skin effect coefficient, and κ_{prox} is the proximity effect coefficient, R_{s_DC} is phase DC resistance.

Incorporating AC losses from (2), the K_m is expressed as:

$$K_m = K_t \Big/ \sqrt{(1+\kappa_{skin} + \kappa_{prox}) R_{s\_DC}} \tag{3}$$

To provide a comprehensive evaluation of energy conversion, a new K_m, including iron and copper losses, was proposed [15]. Applying it here, an updated version integrating AC copper losses is expressed as:

$$K^{up}_{m\_new} = K_t \Big/ \left[\left(\frac{AP_{Iron} + BP^2_{Iron}}{C - AP_{Iron}} + 1 \right) \sqrt{R_{s\_AC}} \right] \tag{4}$$

In which, $A = \lambda_m^3 \omega_e$, $B = L_d L_q i_q$, and $C = i_q \omega_e^2 \lambda_m^4$ (5)

where $K^{up}_{m\_new}$ is the updated motor constant, λ_m is PM flux linkage, λ_d and λ_q are flux linkages, L_d and L_q are inductances in d- and q-axes, and i_d and i_q are d- and q-axis currents.

Increasing the pole numbers improves PD (kW/kg) by reducing yoke thickness, thinning the stator, and enhancing air gap flux density. Then, the electromagnetic power (P_e) at the air gap can be expressed as [15]

$$P_e = \frac{\pi}{2P} B_{g1} K_{s1} \left(D_{IS}^2 L_{stack} \right) \omega_e \tag{6}$$

where B_{g1} is peak air gap flux density, K_{s1} is peak stator surface current density, D_{IS} is inner stator diameter, L_{stack} is active stack length, and ω_e is angular speed.

And $$K_{s1} = \frac{6 k_w N_s I_s}{\pi D_{IS}} \tag{7}$$

where k_w is the winding factor, and N_s is the number of turns/hairpin layers.

Then, the machine sizing can be determined as

$$D_{IS}^2 L_{stack} = 2P \frac{P_e}{B_{g1} K_{s1} \omega_e} \tag{8}$$

Therefore, the T_e as a function of $D_{IS}^2 L_{stack}$ is expressed as

$$T_e = \frac{\pi}{4} \left(D_{IS}^2 L_{stack} \right) B_{g1} K_{s1} \tag{9}$$

Combining equations (2) and (4), the T_e becomes

$$T_e = \frac{3}{2} k_w N_s I_s B_{g1} D_{IS} L_{stack} = K_t I_s \tag{10}$$

Finally, combining (2), (4), and (10), $K^{up}_{m\_new}$ is calculated as

$$K^{up}_{m\_new} = \frac{\left(\frac{3}{2} k_w N_s B_{g1} D_{IS} L_{stack} \right)}{\left[\left(\frac{AP_{Iron} + BP^2_{Iron}}{C - AP_{Iron}} + 1 \right) \sqrt{(1 + \kappa_{skin} + \kappa_{prox}) R_{s\_DC}} \right]} \tag{11}$$

For efficiency calculations, DC copper, iron, and PM eddy current losses are considered [14, 16]

$$\eta = \frac{P_e}{P_{Cu} + P_{Iron} + P_{Edd} + P_e} \times 100\% \tag{12}$$

The DC copper loss, P_{Cu}, is then determined by [14, 16]

$$P_{Cu} = \frac{3}{2} I_s^2 R_{s\_DC} \tag{13}$$

The overall expression of iron losses is provided by [14, 16]

$$P_{Iron} = \left[K_h f B^\beta + K_f K_e f^2 B^2 \right] \tag{14}$$

where K_h is the hysteresis constant, f is the excitation frequency, B is the peak flux density, β is the Steinmetz constant, K_f is the stacking factor, and K_e is the eddy current constant.

The eddy current loss in the PM can be determined [16]

$$P_{Edd} = J_{Edd} / \sigma \tag{15}$$

where J_{Ed} is eddy current density, σ is the electrical conductivity of PM material.

C. Two-Level Optimization Strategy

To maximize the PD and efficiency of the proposed 1 MW-class PM machine, a two-level optimization approach is presented (Fig. 2). This approach focuses on two objectives: 1. maximizing PD and efficiency for both Litz wire and hairpin windings, and 2. minimizing copper loss in the hairpin windings to improve efficiency. The details of the optimization process are outlined below.

The objective function $f(X)$ defining the optimization goal is expressed as:

$$f(X) = \max(PD) - \omega(P_{Cu}) \quad (16)$$

where *max(PD)* maximizes power density, P_{cu} minimizes copper loss, and ω is the weighting factor.

Then, the GO function aims to maximize *PD* as follows:

$$f_{global}(X_G) = \max(P_e / M_{total}) \quad (17)$$

where M_{total} is the total active mass, and X_G is the input design variable.

$$X_G = \{D_{OS}, D_{IS}, S_{wid}, S_{dep}, g, J, N_S, h_C, b_C, PM_{Thick}\} \quad (18)$$

where D_{OS} is the outer stator diameter, S_{wid} is the slot width, S_{dep} is the slot depth, g is the air-gap length, J is the current density, PM_{Thick} is the Halbach PM thickness, and b_C and h_C are the conductor width and height, respectively.

The LO function aims to minimize the copper loss as follows:

$$f_{local}(X_L) = \min(P_{Cu}) \quad (19)$$

The input design variables of X_L are determined as follows:

$$X_L = \{K^{up}_{m\_new}, S_Y, A_S, b_C, h_C\} \quad (20)$$

where S_Y is the stator yoke thickness, A_S is the slot cross-sectional area.

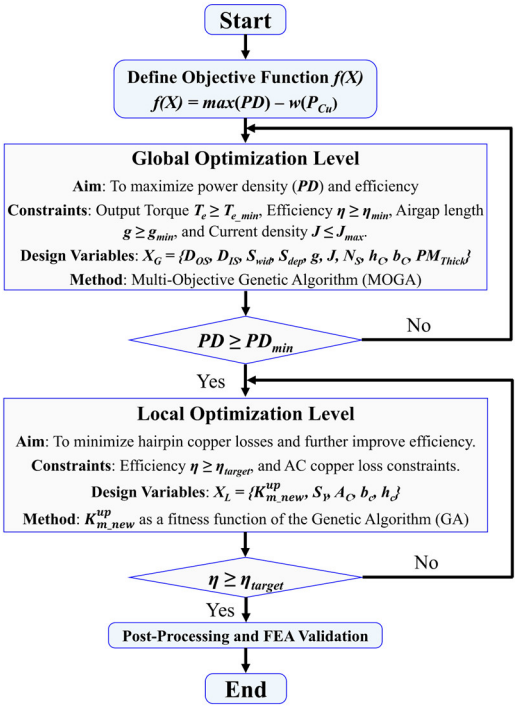

Fig. 2. Flowchart of the two-level optimization strategy.

To support the optimization process, the design variables and optimization range for both GO and LO levels are identified and presented in Fig. 3 and Table II.

III. Optimization Results

A. Global Optimization Results

As discussed, global optimization is implemented to maximize PD and efficiency for both models using Litz wire and hairpin winding. MOGA was applied with 10 generations and a population of 150, evaluating over 1,000 design cases. Optimization results for 1MW-class PM machines with Litz wire and hairpin winding are shown in Figs. 4-6.

Fig. 4 compares PD and efficiency between the two machines at their optimum points after optimization. Both machines meet the three constraints: air-gap length (5mm), current density (≤30A_{rms}/mm²), and maximizing PD. The Litz wire machine achieves its optimum point with a peak PD of 27 kW/kg at 28.7 A_{rms}/mm² and 98.4% efficiency (Fig. 4a). Meanwhile, the hairpin winding machine reaches its optimum point with a higher PD of 35.8 kW/kg at 27 A_{rms}/mm² and 98% efficiency (Fig. 4b).

TABLE II
Optimization Parameter Ranges for The Two-Level Optimization

Global Optimization Level			Local Optimization Level		
Parameters	**Min (mm)**	**Max (mm)**	**Parameters**	**Min (mm)**	**Max (mm)**
D_{OS}	-	< 400	S_Y	8	12
S_{wid}	5	9	S_{wid}	6	9
S_{dep}	15	35	S_{dep}	23	27
D_{IS}	230	280	h_C	1.3	1.6
g	5	5	b_C	4.8	6
PM_{Thick}	10	25			
L_{Stack}	80	115			
h_C	1	3			
b_C	4	7			

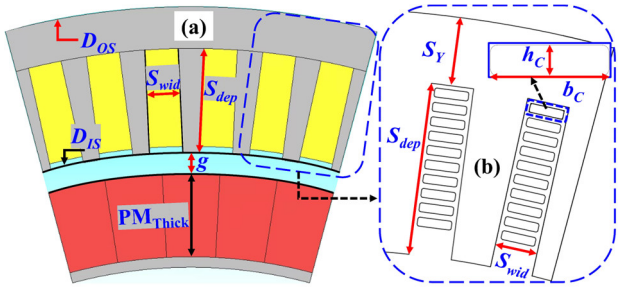

Fig. 3. Design variables for the two-level optimization strategy. (a) Global optimization variable, (b) Local optimization variables.

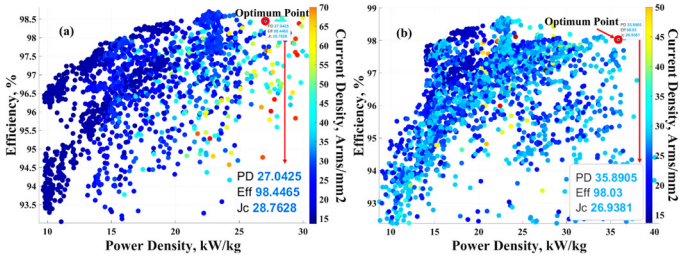

Fig. 4. Global optimization results for power density, efficiency, and current density of (a) Litz wire machine and (b) Hairpin winding machine.

At the optimum point, the hairpin winding machine shows a significant improvement in PD over the Litz wire machine under the same constraints. This is due to its lighter total active mass (stator core, copper winding including end-length, and PM), which is 30 kg compared to the 39.4 kg total active mass of the Litz wire machine, as shown in Fig. 5.

Despite this, at the optimum point, the hairpin winding machine has slightly lower efficiency (98%) than the Litz wire machine (98.4%) under the same constraints. This is mainly due to higher copper losses (19.6 kW) from AC loss in the hairpin winding machine compared to 16.6 kW in the Litz wire machine. However, total losses are not much different (21.6 kW for the hairpin and 19.8 kW for the Litz wire machine), as shown in Fig. 6. The optimization results for both configurations are summarized in Table III. As a result, the

hairpin winding machine achieves over 30% higher PD than the Litz wire machine, with only a 0.4% reduction in efficiency. Further optimizations could enhance the efficiency of the hairpin machine.

TABLE III
SUMMARY OF GLOBAL OPTIMIZATION RESULTS

Optimal design parameters			Optimal design specifications		
Parameters	**Litz wire**	**Hairpin**	**Items**	**Litz wire**	**Hairpin**
D_{OS}	347 mm	320 mm	***PD***	27kW/kg	35.8kW/kg
S_{wid}	8 mm	6 mm	***J***	28.7A_{rms}/mm^2	27 A_{rms}/mm^2
S_{dep}	25.1 mm	22.5 mm	Total losses	19.8kW	21.6kW
D_{IS}	276.4 mm	250 mm	P_{Cu}	16.6kW	19.6kW
g	5 mm	5 mm	M_{total}	39.4kg	30kg
PM_{Thick}	20 mm	23 mm	Efficiency	98.4%	98%
L_{Stack}	103.5 mm	86 mm			
h_C	-	1.5 mm			
b_C	-	5 mm			
A_s	166 mm^2	124 mm^2			

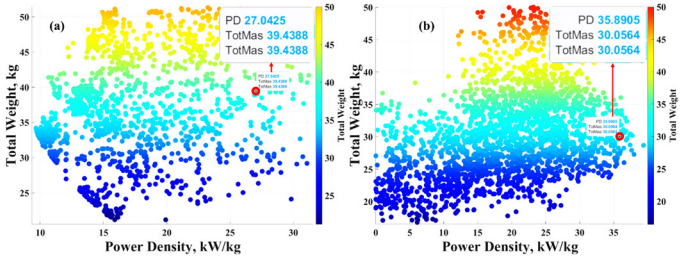

Fig. 5. Global optimization results for power density and total mass of (a) Litz wire machine and (b) Hairpin winding machine.

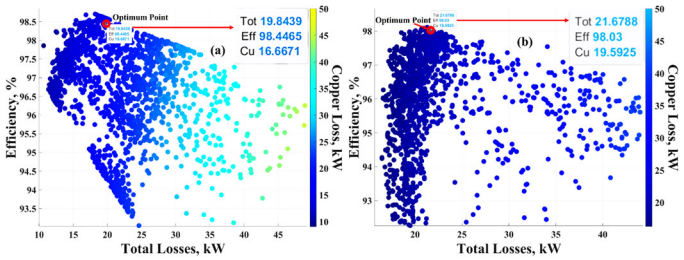

Fig. 6. Global optimization results for efficiency, total losses, and copper loss of (a) Litz wire machine and (b) Hairpin winding machine.

B. *Effect of AC Loss on Hairpin Winding*

As mentioned above, the copper loss in the hairpin winding machine is significantly higher than in the Litz wire machine, primarily due to increased AC loss at high frequencies (1.08 kHz). This AC loss results mainly from skin and proximity effects, caused by leakage flux from stator currents and circulating currents within the hairpin layers due to imbalanced parallel branches. Therefore, this issue requires thorough investigation. In this study, the hairpin winding is designed with 8 layers and 4 parallel branches, each distinguished by different colors, as shown in Fig. 7.

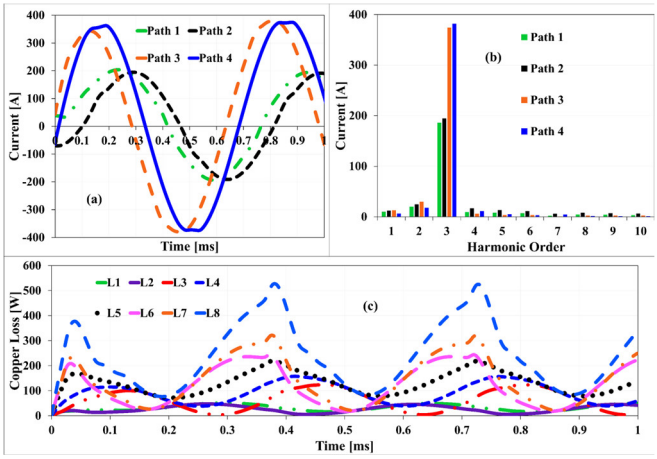

Fig. 8. (a) Distribution of circulating currents between parallel branches, (b) Harmonic distribution of circulating currents, (c) Copper loss distribution across hairpin layers in a slot.

Fig. 8 shows the uneven current distribution across the parallel branches of the hairpin winding machine, with branches near the air gap carrying higher currents. A phase shift between these branches, seen in Fig. 8(a), causes significant third harmonic currents (Fig. 8(b)), increasing core losses. Circulating currents also lead to uneven copper losses, particularly in layers closer to the air gap (L6-L7), as shown in Fig. 8(c).

Fig. 9 compares copper losses in a hairpin winding machine across three scenarios: (1) without AC losses, (2) with AC losses (skin and proximity effects), and (3) with total AC losses, including circulating currents. Copper loss starts at 15.9 kW without AC effects, increases to 19.2 kW with skin and proximity effects, and reaches 21.5 kW with circulating current effects. This highlights the significant impact of AC losses and circulating currents on overall efficiency.

C. *Local Optimization Results*

To enhance the efficiency of the hairpin winding machine, LO optimization is performed using GA with the updated K_m as the fitness function. Table 2 outlines the parameter ranges, while (11) serves as the objective function in JMAG. The GA runs for 20 generations with a population of 100 and 5 offspring per generation, exploring various hairpin dimensions and slot areas. After evaluating over 600 motor constants, $K_{m\_new}^{up}$ converges at 16.6 $Nm/\sqrt{W}$ (Fig. 10(a)), leading to a 0.48% increase in efficiency, reaching 98.48%. This is primarily due

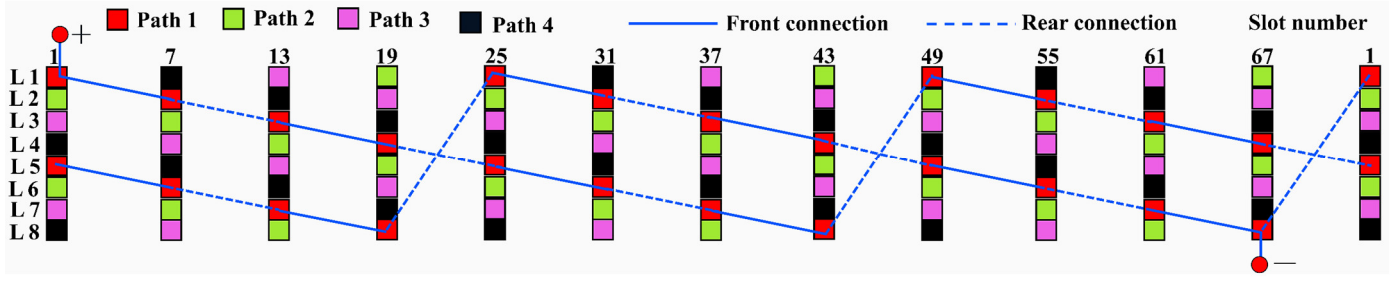

Fig. 7. Winding configurations of 72-slot/12-pole for 1MW-class hairpin winding machine.

to a reduction in copper losses from 21.5 kW (Fig. 9) to 18.37 kW (Fig. 10(b)).

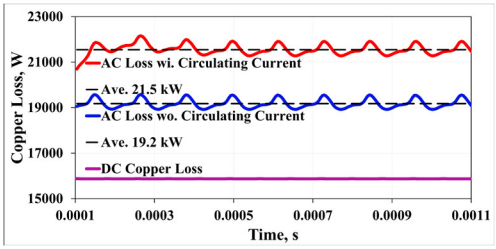

Fig. 9. Copper loss comparison without AC loss, with AC loss due to the skin and proximity effects, and total AC loss.

Figs. 10(b), (c), and (d) illustrate the impact of optimization parameters (S_Y, A_S, h_C, and b_C) on copper and iron losses. At the convergent point of the updated K_m, A_S increases from 124 mm² to 136.17 mm² due to an increase in copper width b_C (5 mm to 5.3 mm) and a reduction in stator yoke S_Y (12 mm to 9.35 mm). While this lowers copper loss in the hairpin winding (from 21.5 kW to 18.37 kW), it slightly increases iron loss.

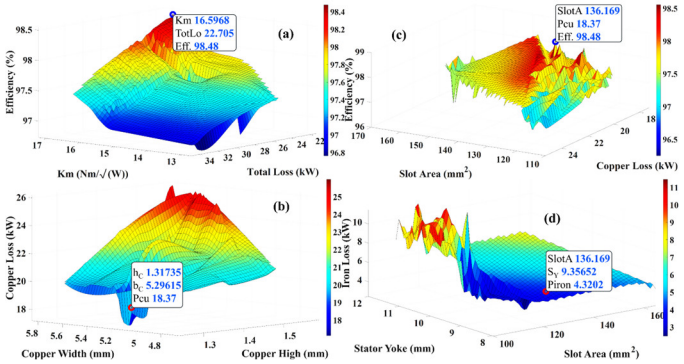

Fig. 10. Local optimization results for the hairpin winding machine. (a) The updated K_m, total losses, and efficiency; (b) Slot area, copper loss, and efficiency; (c) Hairpin conductor size and copper loss; (d) Slot area, stator yoke, and iron loss.

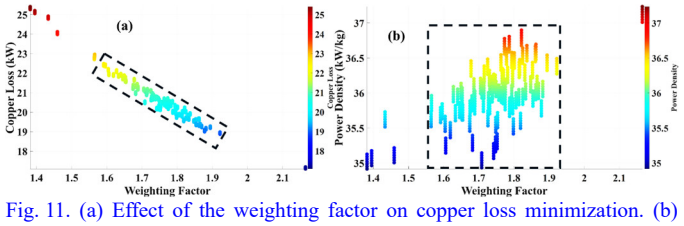

Fig. 11. (a) Effect of the weighting factor on copper loss minimization. (b) Effect of the weighting factor on power density maximization.

The effectiveness of the proposed two-level optimization strategy, which maximizes PD in the GO stage and minimizes copper losses in the LO stage, is ensured by evaluating the weighting factor w (defined in (16)). This factor balances power density and copper loss minimization, as shown in Fig. 11. As the weighting factor increases, copper loss decreases (Fig. 11(a)), while the PD of the hairpin winding reaches its maximum (Fig. 11(b)), confirming the effectiveness of the proposed method.

IV. Conclusion

This paper has presented a two-level optimization strategy for evaluating PD and efficiency in machines with Litz wire and hairpin winding configurations for aircraft propulsion. Two 1 MW-class PM machines, each with a 5-stage Halbach array and a 72-slot/12-pole configuration, are analyzed. The GO stage improves PD and efficiency for both configurations. Hairpin winding increases PD by reducing active mass through shorter stack lengths and end-windings compared to Litz wire. However, high-frequency operation raises AC losses due to skin and proximity effects. The LO optimization, using GA with an updated K_m fitness function, enhances the efficiency of the hairpin winding machine to 98.48%, a 0.48% improvement, by reducing copper losses. The effectiveness of the strategy is validated through FEA.

Acknowledgment

The NEWBORN project is funded by the European Union under Grant Agreement No. 101101967, with UK participants supported by UKRI Grant No. 8219585. The authors thank POWERSYS for providing JMAG software for electric machine design and optimization and for supporting this study.

References

[1] Reducing emissions from aviation. Publications Office of the European Union, 2024. Online Available: https://climate.ec.europa.eu/eu-action/transport/reducing-emissions-aviation_en.

[2] Justin J. Scheidler et al., "Progress Toward the Critical Design of the Superconducting Rotor for NASA's 1.4 MW High-Efficiency Electric Machine," *2019 AIAA/IEEE Electric Aircraft Technologies Symposium* (EATS), Indianapolis, USA, August 2019.

[3] W. Cao et al., "Overview of electric motor technologies used for more electric aircraft (MEA)," *IEEE Trans. Ind. Electron.*, vol. 59, no. 9, pp. 3523–3531, Sep. 2012.

[4] A. Yoon et al., "A high-speed, high frequency, air-core PM machine for aircraft application," in *Proc. IEEE Power Energy Conf.* Illinois (PECI), Feb. 2016, pp. 1–4.

[5] D. Golovanov et al., "4-MW class high-power-density generator for future hybrid-electric aircraft," *IEEE Trans. Transport. Electrific.*, vol. 7, no. 4, pp. 2952–2964, Dec. 2021.

[6] J. Swanke et al., "Comparison of Modular PM Propulsion Machines for High Power Density," in *Proc IEEE Transport. Electrific. Conf. and Expo* (ITEC 2019), Detroit, MI, USA, 08 August 2019.

[7] Glenn Research Center, "Ohio State University Induction Machine," 2023. [Online]. Available: https://www1.grc.nasa.gov/aeronautics/electrified-aircraft-propulsion-eap/eap-for-larger-aircraft/electric-machines/induction-machine/.

[8] R. H. Jansen et al., "Overview of NASA Electrified Aircraft Propulsion Research for Large Subsonic Transports," 2024. [Online]. Available: https://ntrs.nasa.gov/api/citations/20180000402/downloads/20180000402.pdf.

[9] E. K. Mikkelsen et al., "High-Speed MW-Class Generator with Multi-Lane Slotless Winding for Hybrid-Electric Aircraft," *IEEE Access*, vol. 11, 2023.

[10] P. Alvarez et al., "Design of Helical Winding for Slotless Partially Superconducting Electric Machines for Aircraft Propulsion," *IEEE Access*, vol. 12, 2024.

[11] C. Du-Bar and O. Wallmark, "Eddy Current Losses in a Hairpin Winding for an Automotive Application," in *2018 XIII International Conference on Electrical Machines (ICEM),* Alexandroupoli, 2018, pp.710-716.

[12] M. England, B. Dotz, and B. Ponick, "Evaluation of winding symmetry and circulating currents of hairpin windings," in *2021 IEEE International Electric Machines Drives Conference (IEMDC),* 2021, pp. 1–8.

[13] S. Wang et al., "Multilevel Optimization for Surface Mounted PM Machine Incorporating With FEM," *IEEE Trans. Magn.*, vol. 45, no. 10, pp. 4700-4703, October 2009.

[14] D. Hanselman, *Brushless Permanent Magnet Motor Design*, Magna Physics Publishing, ISBN: 1-881855-15-5.

[15] T.A. Huynh, V.H. Che, M.-F. Hsieh, "Maximization of High-efficiency Operating Range of Spoke-type PM E-bike Motor by Optimization through New Motor Constant," *IEEE Trans. Ind. Appl.,* vol. 59, no. 2, pp. 1328 - 1339, 2023.

[16] Lipo, T.A.: *Introduction to AC Machine Design*, 2nd ed. University of Wisconsin Press, Madison (2004).